


 Cite this: *RSC Adv.*, 2020, **10**, 37142

Ab initio study of elastic anisotropies and thermal conductivities of rhenium diborides in different crystal structures

 Yi X. Wang, ^{*a} Ying Y. Liu,^a Zheng X. Yan,^a W. Liu^a and Jian B. Gu^b

The phase stabilities, elastic anisotropies, and thermal conductivities of ReB_2 diborides under ambient conditions have been investigated by using density functional theory calculations. It was found that $P6_3/mmc$ (hP6- ReB_2), $Pmmn$ (oP6- ReB_2), $R\bar{3}m$ (hR3- ReB_2), $R\bar{3}m$ (hR6- ReB_2), and $C2/m$ (mC12- ReB_2) of ReB_2 are both mechanically and dynamically stable, and the order of phase stability is hP6 > oP6 > hR3 > hR6 > mC12. Moreover, the calculated Vickers hardness showed that hP6- ReB_2 , oP6- ReB_2 , hR3- ReB_2 , and mC12- ReB_2 were potential hard materials, while hR6- ReB_2 could not be used as a candidate hard material. In addition, the elastic-dependent anisotropy properties of ReB_2 in different crystal structures were also investigated. The results show that the anisotropic order of the Young's modulus and shear modulus of ReB_2 is hR6 > mC12 > oP6 > hP6 > hR3, while that of the bulk modulus is mC12 > hR3 > hP6 > oP6 > hR6. Finally, by means of Clarke's and Cahill's models, the minimum thermal conductivities of ReB_2 in different crystal structures were further evaluated, and the order of them is hR3 > hP6 > mC12 > oP6 > hR6. Moreover, the results show that all these ReB_2 diborides exhibit relatively low thermal conductivities and are suitable for thermal insulation materials.

 Received 6th September 2020
 Accepted 2nd October 2020

 DOI: 10.1039/d0ra07633c
rsc.li/rsc-advances

1 Introduction

Rhenium borides have attracted great attention in recent years^{1–7} because of their excellent properties such as chemical inertness, high hardness, wear resistance, and electronic conductivity. So far, four binary phases in the system Re–B have been synthesized under environmental conditions, which are Re_3B with orthorhombic phase ($Cmcm$), ReB_3 with hexagonal phase ($P6_3/mmc$), Re_7B_3 with hexagonal phase ($P6_3mc$), and ReB_2 with hexagonal phase ($P6_3/mmc$).^{8–10} Besides, a new monoclinic phase ($C2/m$) of Re_3B was further synthesized under elevated pressure–temperature conditions.¹¹ Meanwhile, other rhenium borides not studied in experiments, such as Re_2B , ReB , Re_2B_3 , Re_3B_7 , Re_2B_5 and ReB_4 , were also reported theoretically.^{6,12–15} Among them, ReB_2 has attracted the most attention due to its interesting properties and ability to be synthesized through a variety of techniques at atmospheric pressure.^{1,2,16–18}

Due to the superior mechanical properties, ReB_2 diborides is a potential hard compound for diverse applications. Therefore, their structural and inner physical properties have been frequently studied theoretically.^{7,15,19–21} In 2007, Wang *et al.*¹⁹ studied the structural, elastic, and electronic properties of ReB_2 by using first-principles calculations. It is found that ReB_2 are

both elastically stable with the hexagonal phase $P6_3/mmc$ (hP6- ReB_2) and orthorhombic phase $Pmmn$ (oP6- ReB_2) under environmental conditions, and the former was more stable than the latter. Moreover, their study showed that ReB_2 is potentially superhard material on the basis of its large bulk moduli and large shear to bulk modulus ratios. Meanwhile, Zhao *et al.*¹⁵ studied the phase stability of ReB_2 under pressure by using density functional theory and found that hP6- ReB_2 is the most stable phase up to 100 GPa. Later, Zhong *et al.*²⁰ investigated the lattice parameters, total energies and mechanical stability of ReB_2 in eight possible crystal structures by performed first-principles calculations. The eight potential ReB_2 structures were based on the known transition metal and light element compounds. They found that the ReB_2 -type (hP6- ReB_2) will transition to MoB_2 -type (hR6- ReB_2) of ReB_2 at about 272 GPa. Furthermore, Mażdziarz *et al.*⁷ investigated the structural and inner physical properties of ReB_2 polymorphs by using density functional theory calculations, which found that $P6_3/mmc$ (hP6- ReB_2), $Pmmn$ (oP6- ReB_2) and $R\bar{3}m$ (hR3- ReB_2) are both mechanically and dynamically stable at ambient conditions. However, due to previous studies only using some known structures in transition-metal diborides to study the structures stability of ReB_2 at ambient conditions and high pressure, the results obtained were not comprehensive. Therefore, we employed the particle swarm optimization (PSO) algorithm to investigate the crystal structure of ReB_2 under different pressures,²¹ and found that hP6- ReB_2 , oP6- ReB_2 , hR3- ReB_2 , hR6- ReB_2 , and monoclinic phase $C2/m$ (mC12- ReB_2) both had

^aCollege of Science, Xi'an University of Science and Technology, Xi'an 710054, People's Republic of China. E-mail: lsdwyx@163.com

^bSchool of Materials and Chemical Engineering, Zhongyuan University of Technology, Zhengzhou, People's Republic of China



relatively low enthalpy at zero pressure, indicating that these phases might be metastable structures of ReB_2 at ambient conditions.

As mentioned above, five structures in hP6, oP6, hR3, hR6, and mC12 of ReB_2 have been reported at ambient conditions. However, so far, their inner physical properties have not been systematically investigated. Since elastic anisotropy is an important factor affecting the mechanical stability of materials, and thermal conductivity is of great significance for its high temperature application. Therefore, in order to acquire a thorough comprehension about the ReB_2 diborides at ambient conditions, we revisit their inner physical properties, especially

the elastic anisotropies and thermal conductivity by using first-principles calculations within the density functional theory (DFT) in this work. Our research results are expected to provide beneficial guidance for the experimental and theoretical work of ReB_2 diborides in the future.

2 Theoretical method and computation details

Ab initio calculations in the framework of density functional theory (DFT) were carried out with the CASTEP code^{22,23} with a Perdew–Burke–Ernzerhof (PBE)²⁴ exchange–correlation

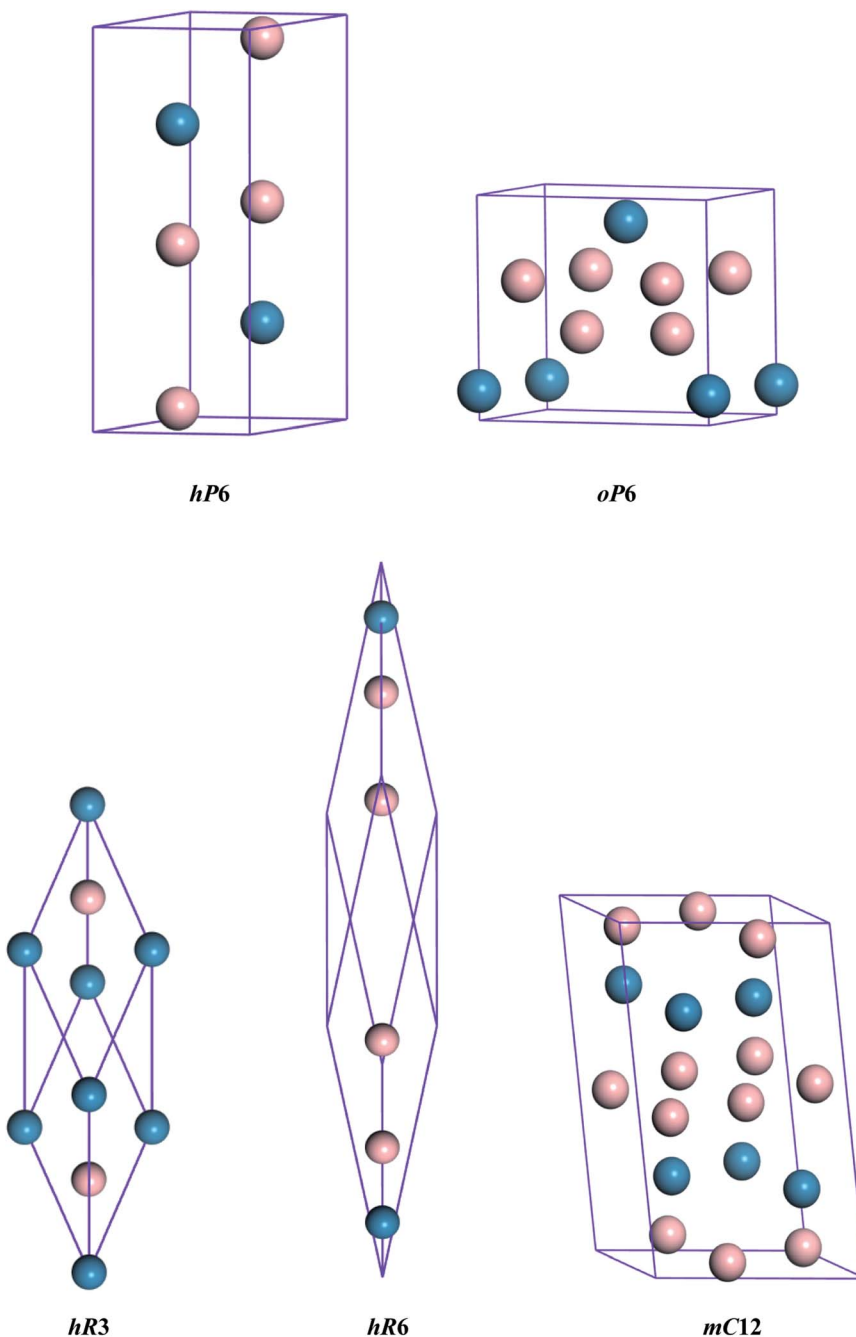


Fig. 1 Crystal structures of ReB_2 . The blue and pink spheres represent the Re and B atoms, respectively.



functional form of the generalized gradient approximation (GGA). The ultrasoft pseudopotential was employed to describe the electron-ion interactions with $5s^25p^65d^56s^2$ and $2s^22p^1$ treated as valence electrons for Re and B atoms, respectively. The kinetic energy cutoff for the plane-wave basis set was 600 eV, and the Monkhorst-Pack k -point meshes were $16 \times 16 \times 6$ for conventional cells of hP6-ReB₂, $8 \times 13 \times 9$ for conventional cells of oP6-ReB₂, $16 \times 16 \times 16$ for conventional cells of hR3-ReB₂, $16 \times 16 \times 16$ for conventional cells of hR6-ReB₂, and $4 \times 12 \times 17$ for conventional cells of mC12-ReB₂, respectively. The tolerances for the geometry optimisation are 5×10^{-6} eV per atom for energy and 0.01 eV Å⁻¹ for force. For phonon calculations, the finite displacement method²⁵ was employed within the CASTEP code. The supercell of all ReB₂ diborides defined by cutoff radius of 5.0 Å. Moreover, the force calculations were conducted with $10 \times 10 \times 4$, $5 \times 9 \times 6$, $10 \times 10 \times 10$, $11 \times 11 \times 11$, and $3 \times 9 \times 5$ k -meshes for hP6-ReB₂, oP6-ReB₂, hR3-ReB₂, hR6-ReB₂, and mC12-ReB₂ supercells, respectively. The above calculation parameters were carefully checked to ensure absolute convergence of the total energy.

3 Results and discussion

3.1 Crystal structures and phase stability

The different crystal structures of ReB₂ are presented in Fig. 1. Our calculations start with the structural optimization by minimizing the total energy to obtain their equilibrium lattice constants. The calculated ground state results, along with the available experimental^{3,10} and theoretical data,^{6,7,20,26,27} are given in Table 1. As shown, our calculated lattice parameters a and c of hP6-ReB₂ are within 0.24% and 0.16% of the experimental data of ref. 10, respectively. Moreover, the lattice parameters of other ReB₂ structures are also consistent with the previous theoretical data within an acceptable error of ~1%. This assessment validated the reliability of our calculation method

and demonstrated that our parameter setting is accurate enough to be used in subsequent studies.

In order to evaluate the relative stability of different ReB₂ structures, the dynamic stability is first checked. The calculated phonon dispersion curves of them at 0 GPa are shown in Fig. 2. As shown, all five ReB₂ diborides have no imaginary phonon frequency, indicating that they are dynamically stable under environmental pressure. In addition, the formation enthalpies are further evaluated using α phase of boron and cubic phase ($Fm\bar{3}m$) of rhenium as the reference structures by the equation: $\Delta H = H(\text{ReB}_2) - H(\text{Re}) - 2H(\text{B})$. As shown in Table 1, the obtained formation enthalpies of hP6-ReB₂, oP6-ReB₂, hR3-ReB₂, hR6-ReB₂, and mC12-ReB₂ are all negative. Among them, hP6-ReB₂ possesses the smallest formation enthalpy (-1.25 eV f.u.⁻¹) and is the most energetically stable ReB₂, which is consistent with the previous experimental^{1,10} and theoretical^{7,15,26,28} results. After it, the formation enthalpy of oP6-ReB₂, hR3-ReB₂, and hR6-ReB₂ are -1.04, -1.03, and -0.35 eV f.u.⁻¹, respectively. Meanwhile, mC12-ReB₂ shows the largest formation enthalpy (-0.28 eV f.u.⁻¹), indicating that its stability is the weakest. Therefore, the phase stability order of ReB₂ should be hP6 > oP6 > hR3 > hR6 > mC12.

3.2 Mechanical properties

3.2.1 Elastic constants and Vickers hardness. Since the elastic constants can be used to judge the mechanical stiffness and stability of materials, we further studied the elastic properties of ReB₂ in different crystal structures by using the strain-stress method. The calculated elastic constants, along with the available theoretical data,^{7,19,20,26,29} are given in Table 2. It is obvious that our obtained elastic constants of different ReB₂ structures are in agreement with the other theoretical results. Moreover, for hexagonal structure of hP6-ReB₂, its mechanical stability criteria is:

Table 1 Calculated lattice parameters, cell volume V_0 and formation enthalpies ΔH of ReB₂ in different crystal structures, together with the available experimental (exp.) and theoretical (cal.) data

Lattice parameters (Å)							
Space group	Pearson symbol	a	b	c	V_0 (Å ³)	ΔH (eV per atom)	Ref.
<i>P</i> 6 ₃ / <i>mmc</i>	hP6	2.907	2.907	7.490	54.843	-1.25	This work
		2.894	2.894	7.416	53.790	-1.34	Cal. ⁶
		2.899	2.899	7.435	54.114		Cal. ⁷
		2.900	2.900	7.478	54.464		Exp. ¹⁰
		2.897	2.897	7.472	54.308		Exp. ³
<i>P</i> mmn	oP6	4.619	2.899	4.122	55.205	-1.04	This work
		4.600	2.892	4.094	54.463		Cal. ⁷
		4.582	2.869	4.077	53.595		Cal. ²⁶
$\bar{R}\bar{3}m$	hR3	4.112	4.112	4.112	27.580	-1.03	This work
		4.082	4.082	4.082	26.676		Cal. ⁷
		4.126	4.126	4.126	28.110		Cal. ²⁷
$\bar{R}\bar{3}m$	hR6	7.244	7.244	7.244	53.724	-0.35	This work
		7.251	7.251	7.251	54.359		Cal. ²⁷
		7.173	7.173	7.173	52.083		Cal. ²⁰
<i>C</i> 2/ <i>m</i>	mC12	7.850	2.889	4.903	110.005	-0.28	This work



$$C_{44} > 0, C_{11} - |C_{12}| > 0, (C_{11} + C_{12})C_{33} - 2C_{13}^2 > 0 \quad (1)$$

The mechanical stability criteria for orthorhombic phase of oP6-ReB₂ is:

$$\begin{aligned} C_{ii} > 0, \quad (i = 1, 2, 3, 4, 5, 6), \\ C_{11} + C_{22} + C_{33} + 2(C_{12} + C_{13} + C_{23}) > 0, \\ C_{11} + C_{22} - 2C_{12} > 0, \quad C_{11} + C_{33} - 2C_{13} > 0, \quad C_{22} + C_{33} - 2C_{23} > 0 \end{aligned} \quad (2)$$

For rhombohedral crystals of hR3-ReB₂ and hR6-ReB₂, their mechanical stability can be judged from:

$$\begin{aligned} C_{11} - |C_{12}| > 0, \quad (C_{11} + C_{12})C_{33} - 2C_{13}^2 > 0, \\ (C_{11} - C_{12})C_{44} - 2C_{14}^2 > 0 \end{aligned} \quad (3)$$

For monoclinic phase of mC12-ReB₂, the mechanical stability criteria is:

$$\begin{aligned} C_{ii} > 0, \quad (i = 1, 2, 3, 4, 5, 6), \\ C_{11} + C_{22} + C_{33} + 2(C_{12} + C_{13} + C_{23}) > 0, \\ C_{33} - C_{55}^2 > 0, \quad C_{44}C_{66} - C_{46}^2 > 0, \quad C_{22} + C_{33} - 2C_{23} > 0 \end{aligned} \quad (4)$$

As shown in Table 2, our calculated elastic constants of these ReB₂ structures all satisfy the corresponding criteria of mechanical stability, indicating that they are mechanically stable. In addition, we can find that the C_{33} values of hP6-ReB₂, oP6-ReB₂, hR3-ReB₂, and hR6-ReB₂ are both greater than C_{11} and C_{22} , indicating that their c axis is stiffer than a and b axis. As for mC12-ReB₂, it is very in-compressible along the a axis because its C_{11} is much bigger than C_{22} and C_{33} .

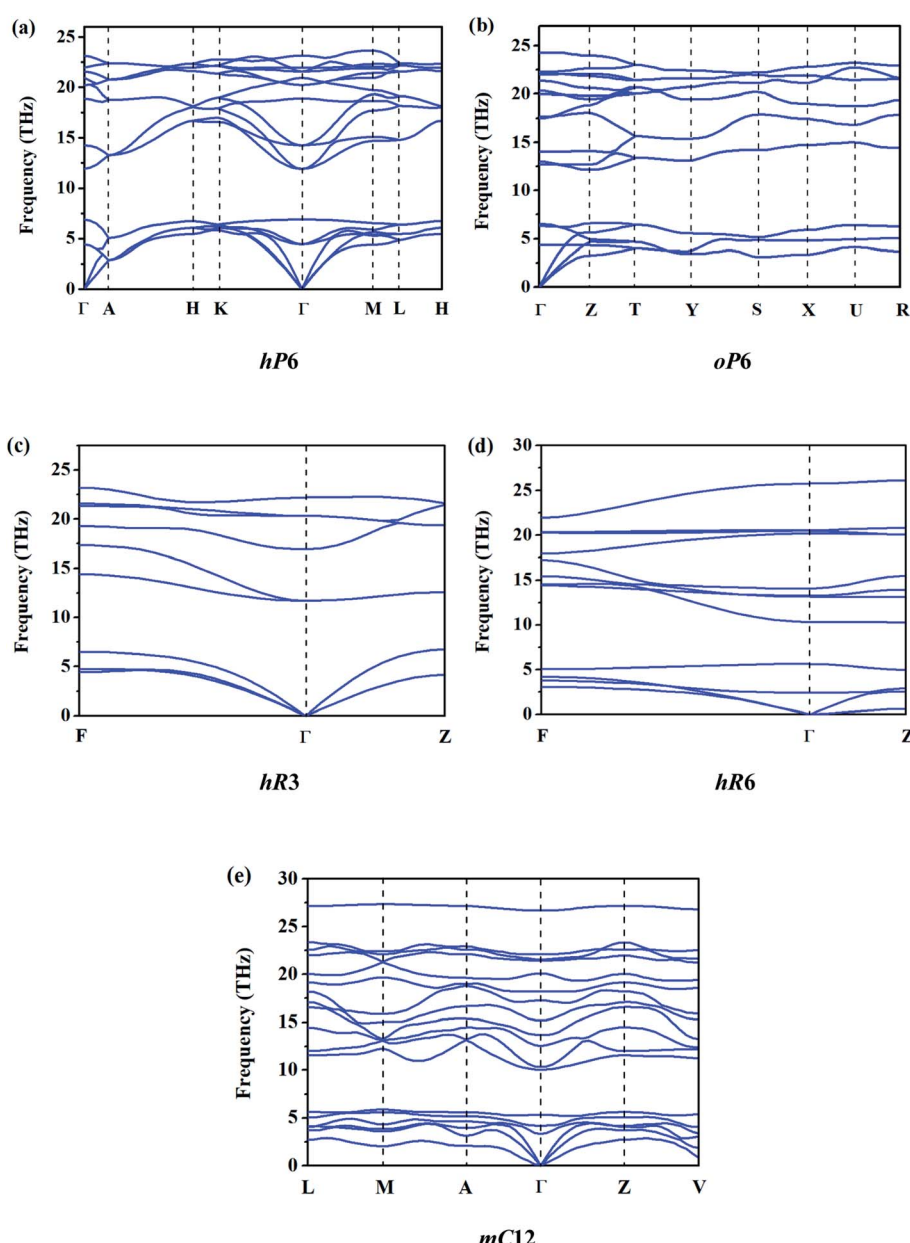


Fig. 2 Calculated phonon dispersion curves of ReB₂ in different crystal structures.



Table 2 Calculated elastic constants C_{ij} (in GPa) and Vickers hardness H_V (in GPa) of ReB_2 in different crystal structures, together with the available theoretical data

Phase	C_{11}	C_{12}	C_{13}	C_{22}	C_{23}	C_{33}	C_{44}	C_{55}	C_{66}	H_V	Ref.
hP6- ReB_2	629	161	124			1011	266		234	38.3	This work
	671	147	137			1040	274		262	40.6	Cal. ⁷
	668	137	147			1063	273		266		Cal. ²⁹
	643	159	129			1035	263		244		Cal. ¹⁹
oP6- ReB_2	598	188	162	618	101	895	206	307	255	35.5	This work
	569	226	173	585	108	923	211	333	248	33.3	Cal. ⁷
	595	208	173	606	100	931	221	331	282	29.3	Cal. ²⁶
hR3- ReB_2	635	144	164			950	285		245	39.3	This work
	649	138	147			997	298		256	41.7	Cal. ⁷
hR6- ReB_2	599	173	226			612	69		213	6.7	This work
	630	160	214			668	81		235		Cal. ²⁰
mC12- ReB_2	955	130	149	629	108	608	207	263	280	38.5	This work

Table 3 Calculated elastic anisotropic indexes (A_U , A_{comp} , A_{shear} , A_1 , A_2 and A_3) of ReB_2 in different crystal structures, together with the available theoretical data

Phase	A_U	A_{comp} (%)	A_{shear} (%)	A_1	A_2	A_3	Ref.
hP6- ReB_2	0.23	1.69	1.93	0.76	0.76	1.00	This work
	0.27			0.74	0.74	1.00	Cal. ³⁹
oP6- ReB_2	0.25	0.88	2.28	0.70	0.94	1.21	This work
hR3- ReB_2	0.20	1.78	1.62	0.91	0.91	1.00	This work
hR6- ReB_2	3.33	0.13	24.99	0.36	0.36	1.00	This work
mC12- ReB_2	0.27	2.25	2.17	0.65	1.03	0.85	This work

Furthermore, it is worth noting that our calculated C_{33} of hP6- ReB_2 , oP6- ReB_2 , and hR3- ReB_2 are 1011, 895, and 950 GPa, respectively. This is comparable to the C_{11} value (\sim 1079 GPa) of diamond,³⁰ suggesting that these ReB_2 diborides may also be potential hard materials. To evaluate the hardness of ReB_2 in different crystal structures, the empirical model proposed by Chen *et al.*³¹ is employed in present work. This model has been successfully applied to a wide range of material systems^{32–35} and it can be expressed as

$$H_V = 2(k^2 G)^{0.585} - 3; k = G/B \quad (5)$$

where G and B is the shear modulus and bulk modulus respectively, which can be deduced from the Voigt–Reuss–Hill approximation³⁶ by the elastic constants C_{ij} . The calculated Vickers hardness H_V , along with the available theoretical data,^{7,26} are also given in Table 2. As shown, our calculated Vickers hardness of hP6- ReB_2 , oP6- ReB_2 , hR3- ReB_2 , and mC12- ReB_2 is 38.3, 35.5, 39.3, 8.5, and 38.5 GPa, respectively, which is consistent with the other theoretical results. Moreover, our results showed that hP6- ReB_2 , oP6- ReB_2 , hR3- ReB_2 , and mC12- ReB_2 are both potential hard materials, where hR6- ReB_2 can not be used as candidate hard materials. From the above, the hardness order of ReB_2 is hR3 > mC12 > hP6 > oP6 > hR6.

3.2.2 Anisotropic properties. As shown in Table 2, there is a relationship of $C_{11} = C_{22} \neq C_{33}$ for hP6- ReB_2 , hR3- ReB_2 , and hR6- ReB_2 , while that for oP6- ReB_2 and mC12- ReB_2 is $C_{11} \neq C_{22}$

$\neq C_{33}$, indicating that the elastic constants of these ReB_2 diborides are anisotropic. Since the anisotropy of elastic constants will result in different mechanical properties of materials in different directions, it is of great significance to fully describe such anisotropic behavior for understanding the mechanical properties of materials. To do so, we can use the elastic anisotropic index (A_U),³⁷ as well as the percentages of compression anisotropy (A_{comp}) and shear anisotropy (A_{shear}),³⁸ to describe the elastic anisotropy of solid. For elastic isotropic crystals, the values of A_U , A_{comp} and A_{shear} are equal to zero. Other values suggest the elastic anisotropy degree of the crystal. In Table 3, the calculated anisotropy indices A_U , A_{comp} , and A_{shear} of ReB_2 in different crystal structures are listed. As shown, our calculated A_U of hP6- ReB_2 is 0.23, which is consistent with the theoretical assessment of 0.27 in ref. 39. Moreover, the results show that hR6- ReB_2 ($A_U \sim 3.33$) has the highest elastic anisotropy and hR3- ReB_2 ($A_U \sim 0.20$) possesses the lowest elastic anisotropy. Thus, the order of elastic anisotropy of ReB_2 should be hR6 > mC12 > oP6 > hP6 > hR3. This order can also be reflected by A_{shear} values. In addition, the calculated maximum value ($\sim 2.25\%$) and minimum value ($\sim 0.13\%$) of A_{comp} belongs to mC12- ReB_2 and hR6- ReB_2 , respectively, which means that mC12- ReB_2 has the highest compression anisotropy, while hR6- ReB_2 has the lowest compression anisotropy. Therefore, the order of compression anisotropy of ReB_2 is mC12 > hR3 > hP6 > oP6 > hR6.

Besides, the elastic anisotropy can also be weighted by shear anisotropic factors. The anisotropic factor A_1 in the (100) plane between [011] and [010] directions, A_2 in the (010) plane between [101] and [001] directions, and A_3 in the (001) plane between [110] and [010] directions can be expressed as⁴⁰

$$A_1 = \frac{4C_{44}}{C_{11} + C_{33} - 2C_{13}}, \quad A_2 = \frac{4C_{55}}{C_{22} + C_{33} - 2C_{23}},$$

$$A_3 = \frac{4C_{66}}{C_{11} + C_{22} - 2C_{12}} \quad (6)$$

For isotropic crystals, the shear anisotropy factors A_1 , A_2 , and A_3 are always equal to 1. A deviation indicates the anisotropy of



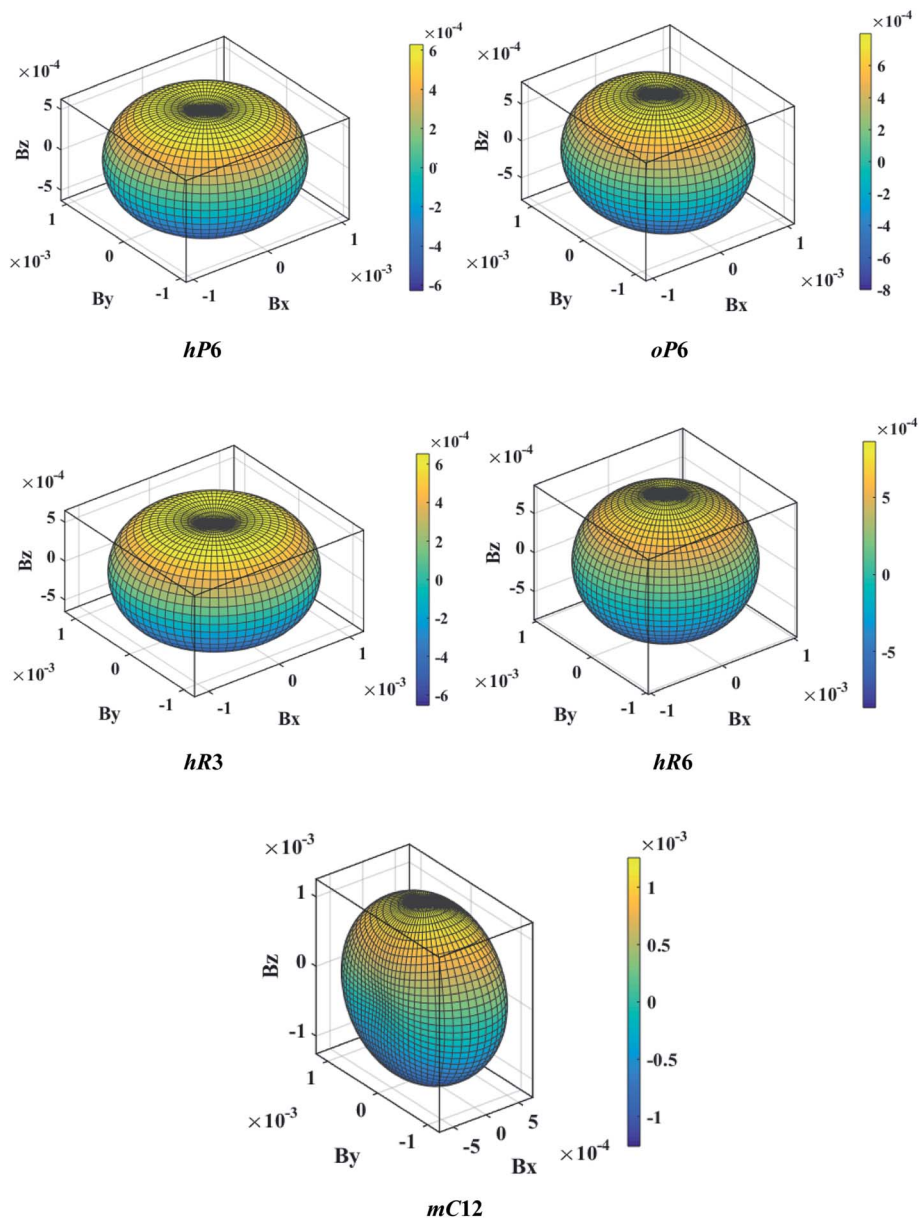


Fig. 3 The direction-dependent bulk modulus of ReB_2 in different crystal structures.

the crystal. The calculated A_1 , A_2 , and A_3 of different ReB_2 structures are also presented in Table 3. As shown, our calculated A_1 , A_2 , and A_3 of hP6- ReB_2 are 0.76, 0.76, and 1.00, respectively, which are in good agreement with the other theoretical values.³⁹ Moreover, the calculated A_1 and A_2 of hR6- ReB_2 deviate more significantly from 1, indicating that it shows the highest shear anisotropy in the (100) and (010) planes. Further, it can be seen that the calculated A_3 of hP6- ReB_2 , hR3- ReB_2 , and hR6- ReB_2 is equal to 1, which means that these three ReB_2 structures are both shear isotropy in the (001) plane. Meanwhile, the absolute value of $(A_3 - 1)$ for oP6- ReB_2 is larger than that for mC12- ReB_2 , suggesting that oP6- ReB_2 has higher shear anisotropy in the (001) plane.

Another better method to study the mechanical anisotropy of materials is to use the directional bulk modulus B , Young's

modulus E , and shear modulus G . These three direction-dependent quantities can be expressed as^{41,42}

$$B = [(S_{11} + S_{12} + S_{13})l_1^2 + (S_{12} + S_{22} + S_{23})l_2^2 + (S_{13} + S_{23} + S_{33})l_3^2]^{-1} \quad (7)$$

$$E = (l_1^4 S_{11} + 2l_1^2 l_2^2 S_{12} + 2l_1^2 l_3^2 S_{13} + l_2^4 S_{22} + 2l_2^2 l_3^2 S_{23} + l_3^4 S_{33} + l_2^2 l_3^2 S_{44} + l_1^2 l_3^2 S_{55} + l_1^2 l_2^2 S_{66})^{-1} \quad (8)$$

$$G = \left[2S_{11}l_1^2(1 - l_1^2) + 2S_{22}l_2^2(1 - l_2^2) + 2S_{33}l_3^2(1 - l_3^2) - 4S_{12}l_1^2l_2^2 - 4S_{13}l_1^2l_3^2 - 4S_{23}l_2^2l_3^2 + \frac{1}{2}S_{44}(1 - l_1^2 - 4l_2^2l_3^2) + \frac{1}{2}S_{55}(1 - l_2^2 - 4l_1^2l_3^2) + \frac{1}{2}S_{66}(1 - l_3^2 - 4l_1^2l_2^2) \right]^{-1} \quad (9)$$



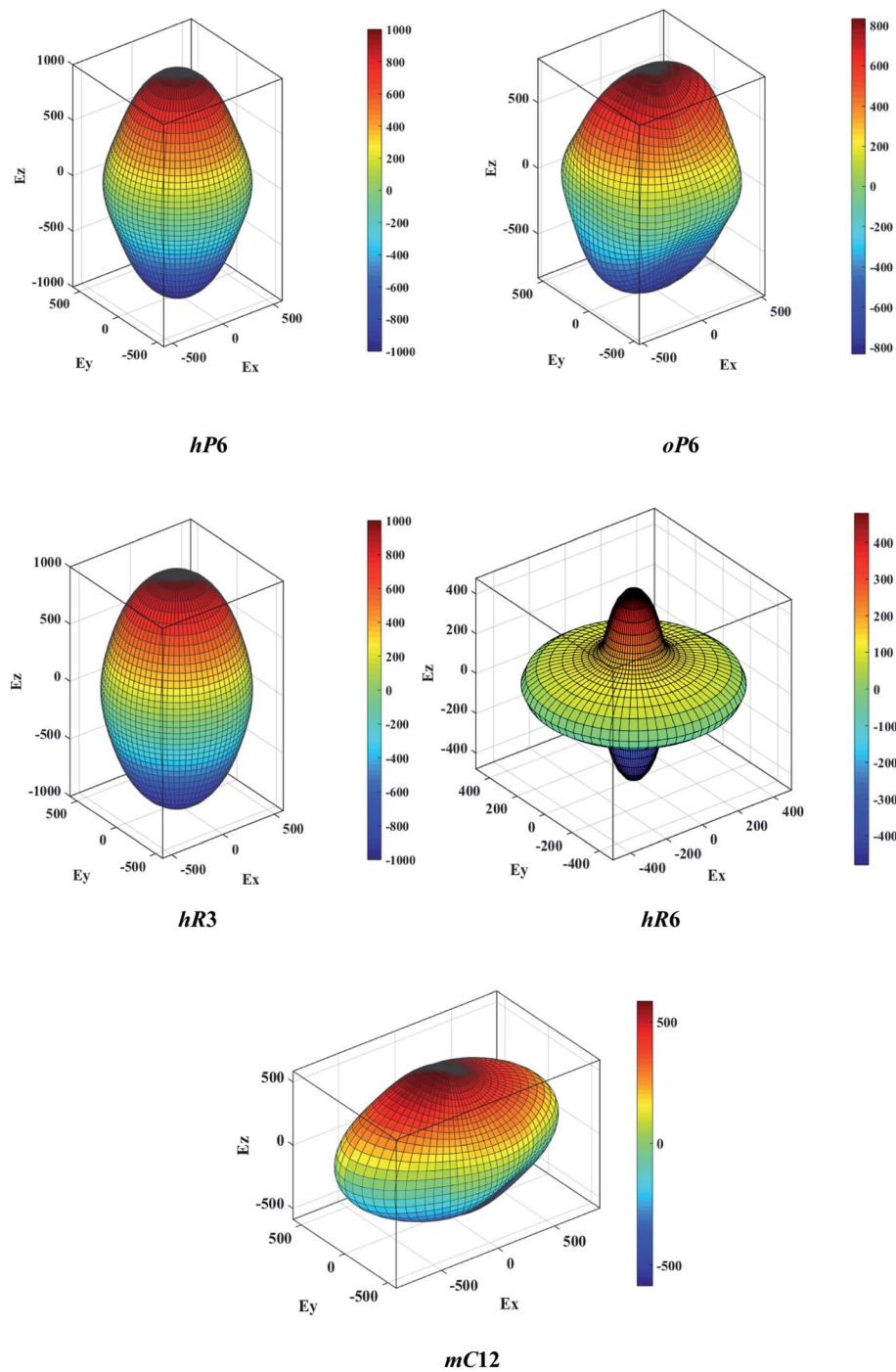


Fig. 4 The direction-dependent Young's modulus of ReB_2 in different crystal structures.

The above three formulas can be used for any crystal system, where l_1 , l_2 , and l_3 are the direction cosines, and S_{ij} are the elements in the compliance tensor. The directional bulk modulus, Young's modulus, and shear modulus of ReB_2 in different crystal structures are plotted in Fig. 3–5, respectively. As shown in Fig. 3, the bulk modulus of different ReB_2 structures in three-dimensional diagrams are not spherical, indicating that their bulk modulus are all anisotropic. According to the deviation degree from the sphere, we can know that mC12-

ReB_2 and hR6- ReB_2 exhibit the largest and least anisotropic of bulk modulus, respectively, which is consistent with our above analysis on A_{comp} . As for Young's modulus (see Fig. 4) and shear modulus (see Fig. 5), the hR6- ReB_2 shows the most remarkable anisotropic nature, followed by mC12- ReB_2 , oP6- ReB_2 , and hP6- ReB_2 , and the last for hR3- ReB_2 . Therefore, the anisotropic order of Young's modulus and shear modulus of ReB_2 is hR6 > mC12 > oP6 > hP6 > hR3, which is in good agreement with the results of A_{U} and A_{shear} .



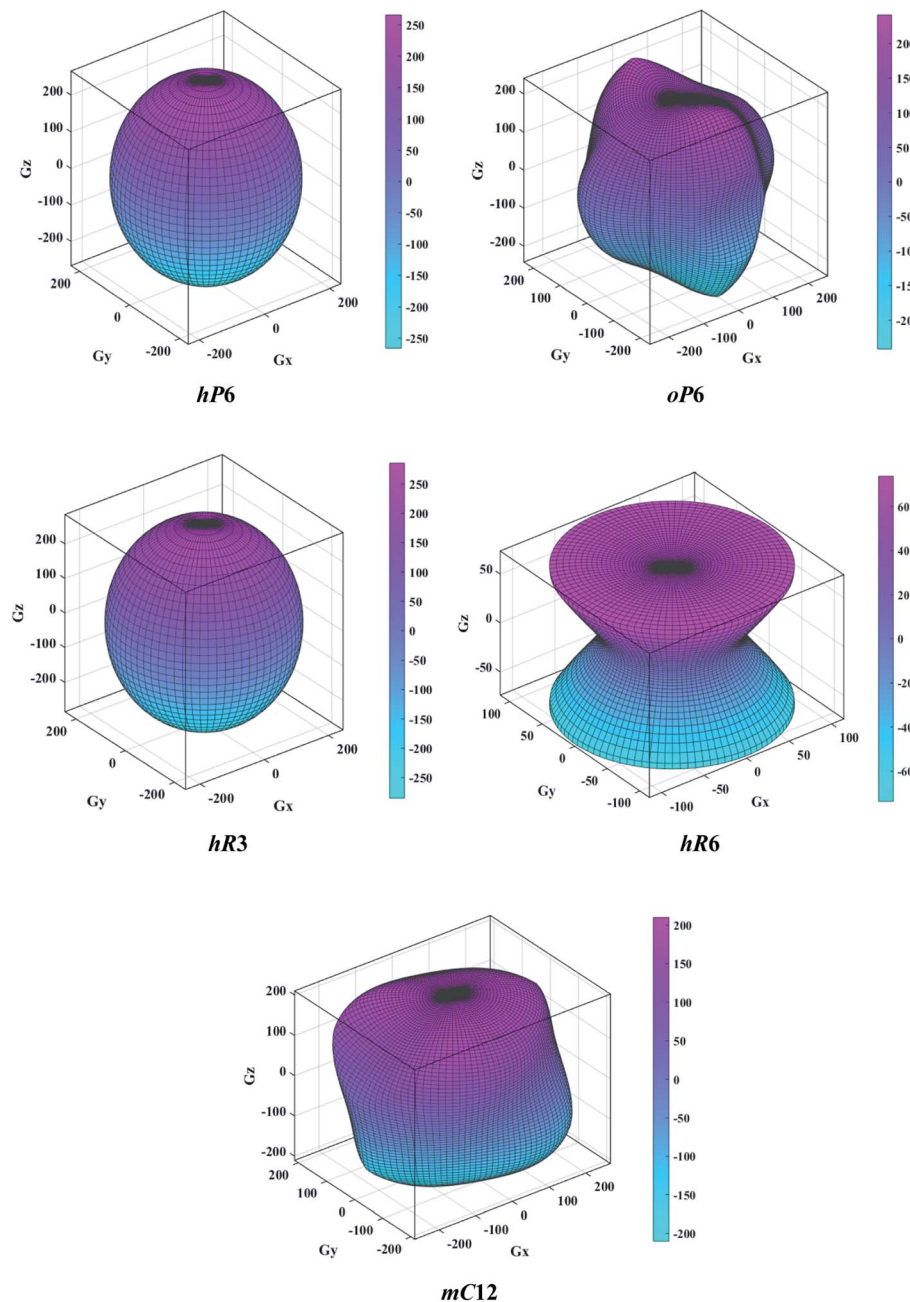


Fig. 5 The direction-dependent shear modulus of ReB_2 in different crystal structures.

Table 4 The density ρ , transverse sound velocity v_t , longitudinal sound velocity v_l , average sound velocity v_m , Debye temperature Θ , Poisson's ratio σ , and Grüneisen parameter γ of ReB_2 in different crystal structures

Phase	ρ (g cm $^{-3}$)	v_t (km s $^{-1}$)	v_l (km s $^{-1}$)	v_m (km s $^{-1}$)	Θ (K)	σ	γ
hP6- ReB_2	12.58	3.29	5.28	3.62	515.78	0.182	1.22
oP6- ReB_2	12.50	3.21	5.20	3.55	503.72	0.191	1.25
hR3- ReB_2	12.51	3.33	5.34	3.66	520.80	0.185	1.23
hR6- ReB_2	12.85	2.26	4.48	2.55	363.70	0.342	2.07
mC12- ReB_2	12.55	3.25	5.19	3.58	508.72	0.178	1.20



3.3 Debye temperatures and thermal conductivities

Debye temperature is an important fundamental parameter that is closely related to the specific heat and melting temperature of solid, and it can be deduced from the following formula⁴³

$$\Theta = \frac{h}{k_B} \left[\frac{3n}{4\pi} \left(\frac{N_A \rho}{M} \right) \right]^{\frac{1}{3}} v_m \quad (10)$$

where h is the Planck constant, k_B is the Boltzmann constant, N_A is the Avogadro number, n is the number of atoms per formula unit, M is the molecular mass per formula unit, ρ is the density, v_m is the average sound velocity and it can be obtained from

$$v_m = \left[\frac{1}{3} \left(\frac{2}{v_t^3} + \frac{1}{v_l^3} \right) \right]^{\frac{1}{3}} \quad (11)$$

According to Navier's equations,⁴⁴ the transverse sound velocity v_t and longitudinal sound velocity v_l can be estimated by

$$v_t = \left(\frac{G}{\rho} \right)^{\frac{1}{2}}, \quad v_l = \left(\frac{3B + 4G}{3\rho} \right)^{\frac{1}{2}} \quad (12)$$

Then, Poisson ratio σ and Grüneisen parameter γ can be calculated as follows:^{45,46}

$$\sigma = \frac{1 - 2(v_t/v_l)^2}{2 - 2(v_t/v_l)^2}, \quad \gamma = \frac{3}{2} \left(\frac{1 + \sigma}{2 - 3\sigma} \right) \quad (13)$$

The calculated sound velocities v_t , v_l and v_m , Debye temperature Θ , Poisson's ratio σ , and Grüneisen parameter γ of different ReB_2 structures are given in Table 4. As shown, hR3-ReB_2 have the largest average sound velocity v_m and Debye temperature Θ , followed by hP6-ReB_2 , mC12-ReB_2 , and oP6-ReB_2 , and the smallest for hR6-ReB_2 . Usually, a higher Debye temperature implies a larger thermal conductivity. Therefore, hR3-ReB_2 should has the highest thermal conductivity, while hR6-ReB_2 possesses the lowest thermal conductivity. Moreover, it is well known that the higher the Debye temperature, the greater the microhardness of the material. Therefore, the order of microhardness of ReB_2 should be $\text{hR3} > \text{hP6} > \text{mC12} > \text{oP6} > \text{hR6}$. In addition, Poisson's ratio σ can be used as a criterion for ductility/brittleness. As shown in Table 4, our calculated Poisson's ratios of hP6-ReB_2 , oP6-ReB_2 , hR3-ReB_2 , and mC12-ReB_2 are both less than 0.26, which means that they are brittle in nature. Meanwhile, the σ value of hR6-ReB_2 is larger than the critical value, implying its ductile nature. Furthermore, it is known that a large Grüneisen parameter usually reflects a strong crystal anharmonicity. Therefore, the order of crystal anharmonicity of ReB_2 should be $\text{hR6} > \text{oP6} > \text{hR3} > \text{hP6} > \text{mC12}$.

In addition, the minimum thermal conductivities of these ReB_2 diborides are further studied in present work, which is of great significance for their high-temperature application. Two theoretical models proposed by Clarke^{47,48} and Cahill⁴⁹ are used to estimate the minimum thermal conductivities of ReB_2 in

Table 5 Calculated minimum thermal conductivities k_{\min} ($\text{W m}^{-1} \text{K}^{-1}$) of ReB_2 in different crystal structures

Phase	Clarke model		Cahill model	
	$M_a(10^{-25})$	k_{\min}	$n(10^{29})$	k_{\min}
hP6-ReB_2	1.150	1.389	1.094	1.509
oP6-ReB_2	1.150	1.357	1.087	1.475
hR3-ReB_2	1.150	1.480	1.088	1.521
hR6-ReB_2	1.150	1.027	1.117	1.162
mC12-ReB_2	1.150	1.367	1.091	1.484

different crystal structures. The Clarke's model follows Debye approach, assuming that the free path of phonon is equal to the interatomic spacing, which can be expressed as:

$$k_{\min} = 0.87k_B M_a^{-\frac{2}{3}} E^{\frac{1}{2}} \rho^{\frac{1}{6}} \quad (14)$$

$$M_a = \frac{M}{mN_A} \quad (15)$$

where k_B is the Boltzmann's constant, M_a is the average mass per atom in the unit cell, E is the Young's modulus, ρ is the density, M is the molar mass, m is the total number of atoms per unit cell, and N_A is the Avogadro's number. Meanwhile, the Cahill's model is mainly based on the Einstein's model, and it can be expressed as:

$$k_{\min} = \frac{k_B}{2.48} n^{\frac{2}{3}} (v_l + 2v_t) \quad (16)$$

where n is the density of the number of atoms per unit volume, v_l and v_t are the longitudinal and transverse sound velocities, respectively. The calculated minimum thermal conductivities of the different ReB_2 structures are given in Table 5. As shown, the calculated value of k_{\min}^{Clarke} is always slightly less than that of k_{\min}^{Cahill} at a given pressure, which is mainly because Clarke's model does not consider the contributions of optical phonon modes to thermal conductivity. Moreover, it is evident that hR3-ReB_2 had the highest minimum thermal conductivities form both Clarke's and Cahill's model, followed by hP6-ReB_2 , mC12-ReB_2 , and oP6-ReB_2 , while hR6-ReB_2 possessed the lowest minimum thermal conductivities. Therefore, the order of minimum thermal conductivities of ReB_2 is $\text{hR3} > \text{hP6} > \text{mC12} > \text{oP6} > \text{hR6}$, which is in agreement with the results of Debye temperature. Furthermore, our calculations show that these five ReB_2 diborides exhibit relatively low thermal conductivities and are suitable for thermal insulation materials.

4 Conclusions

In conclusion, we have systematically investigated the phase stabilities, elastic anisotropies, and thermal conductivities of ReB_2 in five crystal structures by first-principles calculations. Our calculated lattice parameters a , c and cell volume V_0 are consistent well with other available experimental and theoretical data. The calculation of elastic constants and phonon dispersion curves shows that these five ReB_2 structures are both



mechanically and dynamically stable at ambient conditions. According to the calculated formation enthalpies, the order of phase stability of ReB_2 is $\text{hP6} > \text{oP6} > \text{hR3} > \text{hR6} > \text{mC12}$. Moreover, our calculation shows that the hardnesses of $\text{hP6-} \text{ReB}_2$, $\text{oP6-} \text{ReB}_2$, $\text{hR3-} \text{ReB}_2$, and $\text{mC12-} \text{ReB}_2$ are 38.3, 35.5, 39.3, and 38.5 GPa, respectively, indicating that they are potential hard materials. In addition, all the five ReB_2 structures exhibit elastic anisotropy, and the anisotropic order of Young's modulus and shear modulus should be $\text{hR6} > \text{mC12} > \text{oP6} > \text{hP6} > \text{hR3}$, while that of bulk modulus is $\text{mC12} > \text{hR3} > \text{hP6} > \text{oP6} > \text{hR6}$. Finally, the minimum thermal conductivities of the five ReB_2 structures are further evaluated, and the order of them is $\text{hR3} > \text{hP6} > \text{mC12} > \text{oP6} > \text{hR6}$. Moreover, the results show that these five ReB_2 diborides all exhibit relatively low thermal conductivities and are suitable for thermal insulation materials.

Conflicts of interest

There are no conflicts of interest to declare.

Acknowledgements

This work was supported by the National Natural Science Foundation of China under Grant No. 11904282 and 11747110, and the Doctoral Scientific Research Foundation of Xi'an University of Science and Technology under Grant No. 2018QDJ029, and the Science and Technology Tackling Project of the Education Department of Henan Province under Grant No. 172102210072.

References

- 1 H. Y. Chung, M. B. Weinberger, J. B. Levine, A. Kavner, J. M. Yang, S. H. Tolbert and R. B. Kaner, *Science*, 2007, **316**, 436–439.
- 2 N. Dubrovinskaia, L. Dubrovinsky and V. L. Solozhenko, *Science*, 2007, **318**, 1550.
- 3 J. B. Levine, S. L. Nguyen, H. I. Rasool, J. A. Wright, S. E. Brown and R. B. Kaner, *J. Am. Chem. Soc.*, 2008, **130**, 16953–16958.
- 4 C. S. Lue, Y. F. Tao and T. H. Su, *Phys. Rev. B: Condens. Matter Mater. Phys.*, 2008, **78**, 033107.
- 5 X. Q. Chen, C. L. Fu, M. Kremar and G. S. Painter, *Phys. Rev. Lett.*, 2008, **100**, 196403.
- 6 H. Y. Gou, Z. B. Wang, J. W. Zhang, S. T. Yan and F. M. Gao, *Inorg. Chem.*, 2009, **48**, 581–587.
- 7 M. Mażdziarz and T. Mościcki, *J. Alloys Compd.*, 2016, **657**, 878–888.
- 8 B. Aronsson, E. Stenberg and J. Aselius, *Acta Chem. Scand.*, 1960, **14**, 733–741.
- 9 B. Aronsson, M. Backman and S. Rundqvist, *Acta Chem. Scand.*, 1960, **14**, 1001.
- 10 S. J. La Placa and B. Post, *Acta Crystallogr.*, 1962, **15**, 97–99.
- 11 A. Tyutyunnik, T. Dyachkova, Y. Zaynulin and S. Gromilov, *J. Struct. Chem.*, 2014, **55**, 84–88.
- 12 M. Wang, Y. Li, T. Cui, Y. Ma and G. Zou, *Appl. Phys. Lett.*, 2008, **93**, 101905.
- 13 G. Soto, M. G. Moreno-Armenta and A. Reyes-Serrato, *Comput. Mater. Sci.*, 2008, **44**, 628–634.
- 14 E. J. Zhao, J. P. Wang, J. Meng and Z. J. Wu, *J. Solid State Chem.*, 2009, **182**, 960–965.
- 15 E. Zhao, J. P. Wang, J. Meng and Z. J. Wu, *J. Comput. Chem.*, 2010, **31**, 1904–1910.
- 16 S. Otani, T. Aizawa and Y. Ishizawa, *J. Alloys Compd.*, 1997, **252**, 19–21.
- 17 M. Frotscher, M. Holzel and B. Albert, *Z. Anorg. Allg. Chem.*, 2010, **636**, 1783–1786.
- 18 S. Guo, *J. Eur. Ceram. Soc.*, 2014, **34**, 4443–4449.
- 19 Y. X. Wang, *Appl. Phys. Lett.*, 2007, **91**, 101904.
- 20 M. M. Zhong, X. Y. Kuang, Z. H. Wang, P. Shao, L. P. Ding and X. F. Huang, *J. Alloys Compd.*, 2013, **581**, 206–212.
- 21 Y. X. Wang, Z. X. Yan, W. Liu and G. L. Zhou, *J. Appl. Phys.*, 2019, **126**, 135901.
- 22 M. C. Payne, M. P. Teter, D. C. Allen, T. A. Arias and J. D. Joannopoulos, *Rev. Mod. Phys.*, 1992, **64**, 1045.
- 23 V. Milman, B. Winkler, J. A. White, C. J. Packard, M. C. Payne, E. V. Akhmatkaya and R. H. Nobes, *Int. J. Quant. Chem.*, 2000, **77**, 895–910.
- 24 J. P. Perdew, K. Burke and M. Ernzerhof, *Phys. Rev. Lett.*, 1996, **77**, 3865.
- 25 K. Parlinski, Z. Q. Li and Y. Kawazoe, *Phys. Rev. Lett.*, 1997, **78**, 4063.
- 26 M. M. Zhong, X. Y. Kuang, Z. H. Wang, P. Shao, L. P. Ding and X. F. Huang, *J. Phys. Chem. C*, 2013, **117**, 10643–10652.
- 27 R. F. Zhang, D. Legut, R. Niewa, A. S. Argon and S. Veprek, *Phys. Rev. B: Condens. Matter Mater. Phys.*, 2010, **82**, 104104.
- 28 Y. C. Liang and B. Zhang, *Phys. Rev. B: Condens. Matter Mater. Phys.*, 2007, **76**, 132101.
- 29 X. F. Hao, Y. H. Xu, Z. J. Wu, D. F. Zhou, X. J. Liu, X. Q. Cao and J. Meng, *Phys. Rev. B: Condens. Matter Mater. Phys.*, 2006, **74**, 224112.
- 30 H. J. McSkimin, P. Andreatch and P. Glynn, *J. Appl. Phys.*, 1972, **43**, 985–987.
- 31 X. Chen, H. Niu, D. Li and Y. Li, *Intermetallics*, 2011, **19**, 1275–1281.
- 32 A. Misra and W. Y. Ching, *Sci. Rep.*, 2013, **3**, 1488.
- 33 X. Chen, H. Niu, C. Franchini, D. Li and Y. Li, *Phys. Rev. B: Condens. Matter Mater. Phys.*, 2011, **84**, 121405.
- 34 Y. Liang, Y. Gou, X. Yuan, Z. Zhong and W. Zhang, *Chem. Phys. Lett.*, 2013, **580**, 48–52.
- 35 H. Y. Zhang, F. Xi, Z. Y. Zeng, X. R. Chen and L. C. Cai, *J. Phys. Chem. C*, 2017, **121**, 7397–7403.
- 36 G. V. Sin'ko and N. A. Smirnov, *Phys. Rev. B: Condens. Matter Mater. Phys.*, 2005, **71**, 214108.
- 37 S. I. Ranganathan and M. Ostoja-Starzewski, *Phys. Rev. Lett.*, 2008, **101**, 055504.
- 38 F. W. Vahldiek and S. A. Mersol, *Anisotropy in Single-Crystal Refractory Compound*, Springer, US, 1968.
- 39 M. Marín-Suárez, M. E. Vélez, J. David and M. Arroyave-Franco, *Comput. Mater. Sci.*, 2016, **122**, 240–248.
- 40 P. Ravindran, L. Fast, P. A. Korzhavyi, B. Johansson, J. Wills and O. Eriksson, *J. Appl. Phys.*, 1998, **84**, 4891–4904.
- 41 J. F. Nye, *Physical Properties of Crystals: Their Representation by Tensors and Matrices*, Clarendon Press, Oxford, 1985.



42 R. F. S. Hearmon and A. A. Maradudin, *Phys. Today*, 1961, **14**, 48.

43 O. L. Anderson, *J. Phys. Chem. Solids*, 1963, **24**, 909–917.

44 K. B. Panda and K. S. Ravi Chandran, *Comput. Mater. Sci.*, 2006, **35**, 134–150.

45 Y. L. Pei, J. Q. He, J. F. Li, F. Li, Q. J. Liu, W. Pan, C. Barreteau, D. Berardan, N. Dragoe and L. D. Zhao, *NPG Asia Mater.*, 2013, **5**, 47.

46 Y. Xiao, C. Chang, Y. L. Pei, D. Wu, K. L. Peng, X. Y. Zhou, S. K. Gong, J. Q. He, Y. S. Zhang, Z. Zeng and L. D. Zhao, *Phys. Rev. B*, 2016, **94**, 125203.

47 D. R. Clarke, *Surf. Coatings Technol.*, 2003, **163**, 67–74.

48 D. R. Clarke and C. G. Levi, *Annu. Rev. Mater. Res.*, 2003, **33**, 383–417.

49 D. G. Cahill, S. K. Watson and R. O. Pohl, *Phys. Rev. B: Condens. Matter Mater. Phys.*, 1992, **46**, 6131.

